Geophys. J. Int. (1998) **134,** 889–902

New seismic data support Cenozoic rifting in George VI Sound, Antarctic Peninsula

A. C. Bell and E. C. King

British Antarctic Survey, Madingley Rd, Cambridge, CB3 0ET, *UK. E-mail: acbe@pcmail.nerc-bas.ac.uk*

Accepted 1998 April 7. Received 1998 April 7; in original form 1997 November 25

SUMMARY

New multifold seismic-reflection and wide-angle reflection/refraction data across George VI Sound, Antarctic Peninsula, show the presence of graben and horst structures indicating an extensional origin. The data suggest that rocks of an accretionary complex and fore-arc basin underlie the Sound and are in faulted contact along its eastern boundary with volcanic and plutonic rocks of the associated Mesozoic arc of western Palmer Land. A cover of possible syn- and postglacial Cenozoic deposits drapes the structures. The combination of new seismic, synthetic-aperture radar and previously acquired data suggests subduction-related rifting in the Sound was segmented, with opening in the south predominately by normal extension whilst in the north, dextral transtension predominated.

Key words: Cenozoic rifting, George VI Sound, postglacial sedimentation, rift segmentation, seismic reflection, synthetic-aperture radar.

1 INTRODUCTION

The Antarctic Peninsula is a predominantly Mesozoic magmatic island arc associated with subduction of proto-Pacific seafloor beneath the palaeo-Pacific margin of Gondwana, prior to mid-Jurassic seafloor spreading and break-up. The Antarctic Peninsula forms a southerly continuation of the Andean magmatic province of South America and was created by accretion, magmatism and extensional processes (Barker 1982; Storey & Garrett 1985; Storey & Nell 1988). George VI Sound (GVIS) forms a prominent curvilinear trough on the western side of the Antarctic Peninsula, between Alexander Island and Palmer Land (Fig. 1). The trough is 500 km in length and varies in width from 30 km in the north to between 70 and 90 km in the western dog-leg to the south. An extensive ice shelf covers most of the Sound; previous studies indicate ice thicknesses of 93–505 m and seabed depths of 280–1066 m below mean sea level (Maslanyj 1987).

The region is subdivided into three geological domains (Fig. 2).

(1) The LeMay Group (LMG) is a Mesozoic accretionary complex that crops out along the central spine and western flank of Alexander Island (Burn 1984; Tranter 1991).

(2) The Fossil Bluff Group (FBG) comprises Jurassic–Early Cretaceous fore-arc basin sedimentary rocks, predominantly interbedded shales, sandstones and conglomerates (Butterworth *et al.* 1988; Moncrieff & Kelly 1993). The FBG is exposed on the eastern flank of Alexander Island and forms the western border of GVIS. The Fossil Bluff and LeMay Groups are found in both faulted and unconformable contact on the eastern flank of Alexander Island (Doubleday, Macdonald & Nell 1993; Moncrieff & Kelly 1993).

(3) The eastern border of GVIS comprises Jurassic–Cretaceous arc-related volcanic and magmatic rocks of western Palmer Land (Rowe 1973; Ayling 1984; Leat & Scarrow 1994; Leat, Scarrow & Millar 1995; Wareham, Millar & Vaughan, 1997). The nature of the contact between the FBG and the arc volcanic rocks is obscured below GVIS. Only at Carse Point in western Palmer Land (Fig. 2) are rocks similar to the FBG fore-arc deposits found conformably overlain by andesitic volcanic rocks (Culshaw 1975; Thomson 1975).

The LeMay Group contains rocks of early Jurassic to late Cretaceous ages (Tranter 1991; Holdsworth & Nell 1992); however, the age range of the Group is ambiguous. Fission track ages indicate accretion taking place at middle Jurassic times (Doubleday *et al.* 1993); the deposition continued over the duration of FBG sedimentation (Holdsworth & Nell 1992). FBG deposition in the fore-arc basin started in ?Bathonian–Kimmeridgian and continued into Albian times, 97 Ma ago (Butterworth *et al.* 1988; Doubleday *et al.* 1993; Moncrieff & Kelly 1993). Deformation within the FBG has been attributed to dextral transpression caused by oblique subduction (Nell & Storey 1991), occurring shortly after deposition and possibly coeval with final sedimentation (Doubleday *et al.* 1993). Zircon fission track data, recorded from the previously accreted and buried material, indicate a denudational cooling event extending from mid-Cretaceous (100 Ma) to Cenozoic times. Steady cooling continued before being interrupted by a phase

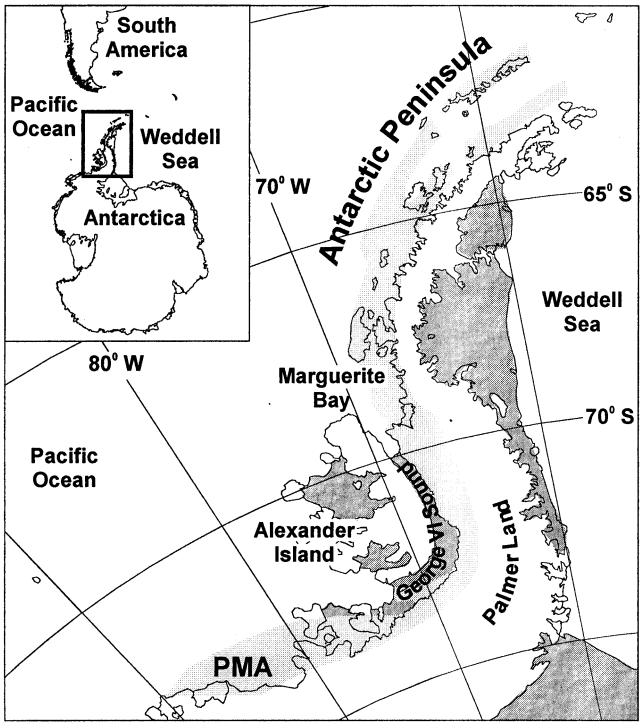

Figure 1. Location map. George VI Sound separates Alexander Island from Palmer Land, southern Antarctic Peninsula. Light grey, Pacific Margin Anomaly (PMA): a large positive magnetic anomaly associated with the Antarctic Peninsula batholith. Dappled grey, ice shelves surrounding the Antarctic Peninsula. Inset shows location of the Antarctic Peninsula with respect to South America and Antarctica.

of accelerated cooling between 40 and 35 Ma, interpreted from analysis of apatite fission track data (Storey *et al.* 1996). Analysis of fission track data from calc-alkaline plutons and volcanic rocks from Alexander Island reveal high-level emplacement (<2 km) between 40 and 60 Ma (Storey *et al.* 1996).

Barker (1982) and Cande, Herron & Hall (1982) record a reduction in subduction rates from 80 to 40 mm yr^{-1} at 50 Ma. Recent analysis of a marine magnetic profile shows a reduction from 102 to 42 mm yr^{-1} at 52.3 Ma (McCarron & Larter 1998) following a clockwise rotation of the angle of subduction from an oblique to more normal orientation at 62 Ma. Recent re-evaluation of the ages of collisions between the Antarctic–Phoenix ridge segments and a former trench at the Antarctic Peninsula margin shows ridge arrival times of 30.1 and 40–44 Ma north and south of the Heezen fracture zone, respectively (Larter *et al.* 1997). These arrival times mark the end of subduction and consequently of subduction-related accretion within the fore-arc of the LeMay Group.

The most probable age of a subduction-related rifting episode within the Antarctic Peninsula fore-arc is between 50 and 30 Ma. During this period the reduction in subduction rates, increased uplift and emplacement of high-level plutons evidence a stress and thermal environment conducive to rifting.

A regional aeromagnetic survey revealed an extensive, smooth negative magnetic anomaly over Alexander Island (Renner, Sturgeon & Garret 1985), which continues to the eastern border of the Sound, where a steep magnetic anomaly gradient marks the western edge of the Pacific Margin Anomaly (PMA) (Fig. 1). The PMA is generally thought to mark the position of an extensive batholith formed during the prolonged period of Mesozoic and Tertiary subduction of proto-Pacific oceanic lithosphere at a trench situated on the western margin of the Antarctic Peninsula (Garrett 1990). The continuation of the smooth negative magnetic anomaly signature across GVIS may indicate a lateral continuation of the magnetically quiet LMG and FBG under the Sound.

Since the first visit to GVIS in 1936 (Fleming *et al.* 1938), speculation as to its origin has focused on a failed rift. A possible age range for the rifting episode spans the early Cretaceous to mid-Tertiary. Supporting evidence for rifting has come from geomorphology (King 1964), structural geology (Storey & Nell 1988), radio echo-soundings (Crabtree, Storey & Doake 1985) and seismic bedrock depth profiles (Maslanyj 1987). An alternative origin as a structurally controlled fluvio-glacial feature was put forward by Nichols (1953).

A seismic traverse across the Sound was undertaken to determine whether the Sound was of tectonic or fluvio-glacial origin, the extent of the FBG under the Sound and the nature of the contact between the fore-arc and arc rocks, and whether any Cenozoic sediment is present beneath the Sound.

2 DATA

2.1 Seismic evidence

During the 1994/5 field season a seismic traverse was undertaken from the Uranus Glacier across GVIS to the Batterbee Mountains (Fig. 2). A total of 23 km of surface-shot multifold reflection line was acquired. An additional, orthogonal short reflection line and walkaway velocity experiment were conducted at the midpoint of the Sound (point W in Fig. 2). Detailed acquisition parameters for the 1994/5 experiments are given in King & Bell (1997).

A typical shot record from a surface-laid charge recorded on GVIS is presented in Fig. 3(a). The surface-laid explosive source produces a sharp, spiked wavelet composed of a dominant compression and rarefaction cycle. The source pulse is approximately seven milliseconds in duration with a frequency bandwidth between 50 and 200 Hz and a dominant frequency of 130 Hz.

Non-dispersive ground roll overprints the primary seabed reflection between 2000 and 2400 m shot offset. Ice-base primary reflection and multiple reverberations within the ice layer ($I_1, I_2, \ldots$) are reduced to a negligible amplitude by the time the primary reflections are recorded. The primary reflections are overprinted by large-amplitude multiple and converted phases generated in the ice and water columns (Beaudoin, ten Brink & Stern 1992; Jarvis & King 1993; King & Bell 1995). Ray trace modelling (Figs 3b and c) identifies the seabed reflection phase conversions and multiples P–P–S, S–P–S and I_2W_1 (see Fig. 3 for explanation of nomenclature). These conversions and short-period ice-layer multiples are most problematical for the interpretation of primary upper-crustal reflections, displaying a similar amplitude, frequency spectrum and moveout velocity. In the preliminary stack of the traverse line (King & Bell 1997), rudimentary data processing left significant residual noise, inhibiting the interpretation.

The high-velocity near-surface ice layer yields a wide subcritical-angle reflection window for subseabed primary reflections. Inclusion of these wide-offset traces in the stack maximizes the primary energy whilst providing the greatest move-out discrimination between the primaries and converted phases/

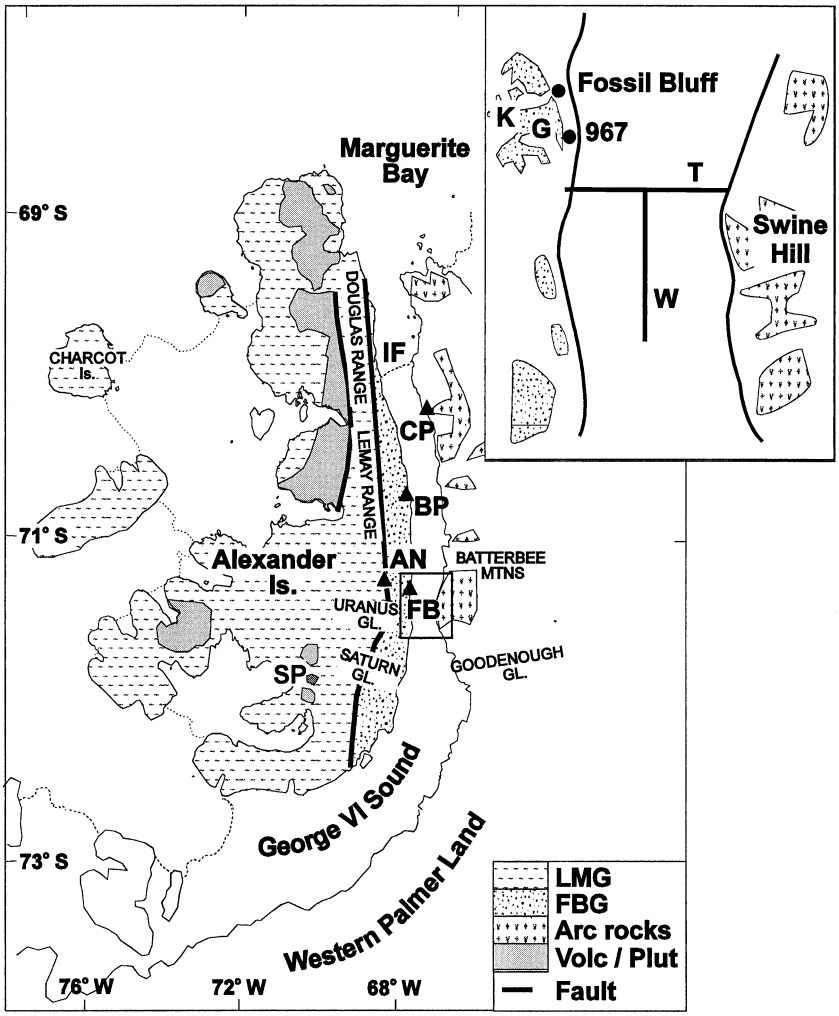

Figure 2. Map illustrating the three main geological domains present in Alexander Island and western Palmer Land. LMG, LeMay Group fore-arc accretionary complex; FBG, Fossil Bluff Group fore-arc basin sediments; Arc rocks, plutonic and volcanic rocks of the Mesozoic arc; Volc/Plut, Cenozoic volcanic and plutonic rocks of Alexander Island; AN, Atoll Nunataks; CP, Carse Point; FB, Fossil Bluff; BP, Belemnite Point; SP, Stacatto Peaks; IF, location of depth soundings performed by Crabtree *et al.* (1985). Extent of ice shelves marked by dotted line. Inset: T, multifold seismic traverse; W, walkaway velocity experiment; 967, location of 1996/7 refraction experiment on the ski-way; K, Khufu Peak; G, Giza Peak.

multiples. The *S–P–S* phase is discriminated against by its lower moveout velocity in comparison to primary reflections and may be reduced by either frequency–wavenumber (FK) filtering or surgical muting in either common shot-point (CSP) or common midpoint (CMP) domains before stacking. Both the I_2W_1 and the *P–P–S* phases may be suppressed by predictive deconvolution and stacking.

In order to retain the wide-offset data in the stack, the move-out correction was calculated using curved-ray-path theory. A method employing the numerical solution of the ray parameter equations was applied, after Grant & West (1965). Fig. 4 illustrates the difference in moveout for a primary seabed reflection event (hyperbola P) at 880 ms zero offset TWT (two-way traveltime) ray traced through an ice shelf velocity function. The overcorrection of wide offsets seen in curve N results from using the standard normal moveout algorithm (Taner & Koehler 1969), whilst curve I illustrates the more accurate moveout correction applied using the ray parameter solution.

Dip moveout was applied to the data prior to stacking. This, together with a post-stack steep-dip time migration, was used to address the effect of steeply dipping seabed bathymetry and subseabed structure. A brief outline of the processing methodology applied to the data is supplied in Table 1.

An additional short-offset refraction experiment was acquired during the 1996/7 field season in order to establish an outcrop velocity for the FBG. The experiment was sited at the Fossil Bluff ski-way (Fig. 2) and lines were orientated parallel and orthogonal to a scarp footwall. A 575 m aperture array comprising single geophones at 25 m intervals was employed. Shots were sited 5 m off the end of the array at one metre depth. Triggering of the recorder was achieved using an uphole geophone.

2.2 Results

2.2.1 Reflection data

The seismic reflection profile across the Sound is shown in Fig. 5. The steep boundary walls produce complex wave fronts not easily imaged with standard software. The better resolution

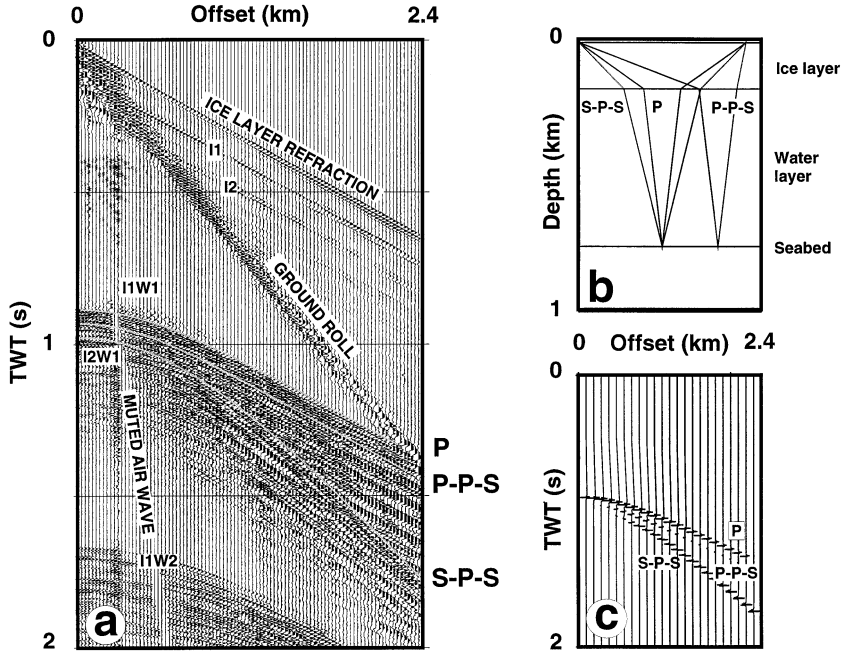

Figure 3. (a) Typical shot record acquired over George VI Sound Ice Shelf. Air wave muting and ground roll attenuation (FK filter) have been applied in order to highlight primary seabed reflection phases (*P*, primary; *P–P–S*, shear wave conversion of primary reflection at the base of the ice layer; *S–P–S*, seabed reflection with ray travelling as an *S*-wave through both traverses of the ice layer). Naming convention for multiple reflections: I_1W_1, primary reflection; I_2W_1, ice-layer multiple (extra bounce in ice layer); I_1W_2, water-layer multiple. (b) Simple modelling of George VI Ice Shelf showing seabed reflection primary and converted-phase ray paths for arrivals at a 2.4 km source offset. The low moveout velocity of the *S–P–S* phase is due to the relatively slow shear wave propagation velocity of ice combined with an extended period spent traversing the water layer. (Layer *P*-wave velocities: ice layer, 1.6/3.79 km s^{-1} (near surface/basal); water layer, 1.48 km s^{-1}; seabed, 3.99 km s^{-1}.) (c) Amplitude modelling of converted phases. Note strong *S–P–S* phase arrivals at far offsets. The *P–P–S* phase is weak relative to the primary reflection.

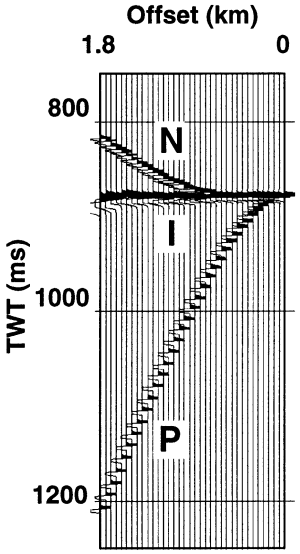

Figure 4. Synthetic CMP gather of a primary seabed reflector below a model of the George VI Ice Shelf, illustrating the improvement in reflection alignment when using a ray parameter algorithm in comparison to standard normal-moveout (NMO) algorithms (P, primary seabed reflection; N, NMO corrected reflection; I, ray-path integral moveout corrected reflection).

of the western boundary wall is due to a more favourable acquisition geometry. In King & Bell (1997) four seismic units were proposed; these are retained for clarity in the following summary of results.

The portion of the Sound between the western boundary wall and kilometre 8.5 is dominated by a graben and a horst, approximately 2.2 and 4.5 km in width, respectively (Fig. 6). Three seismic units (SU1–3) can be identified. Directly below the seabed, SU1 comprises seabed-parallel continuous internal reflectors. The unit varies in thickness, up to a maximum of 45 ms TWT, and drapes both structures. Point diffractors are observed disrupting the subhorizontal reflectors in the western graben; we interpret their origin as entrained boulders released by the Uranus Glacier as it flows into the Sound.

SU2 consists of a band of chaotic and discontinuous weak internal reflectors separating the coherent internal reflectors of SU1 and SU3. The unit exhibits the greatest time thickness in the graben, whilst thinning out and infilling pockets in the faulted topography of the horst.

The positive identification of SU3 as primary intrabasement reflectors, rather than as ice-layer multiples of SU1 (I_2W_1) reflections, is based on the following reasoning. There is no delay between the onset of the two reflector units that is consistent with the two-way traveltime of the ice-layer bounce. The reverse dips between the SU1 reflectors overlying SU3 reflectors are inconsistent with a multiple origin. The SU3 reflectors are laterally disrupted and contain subparallel reflections, in contrast to the laterally consistent parallel reflections within SU1; a more consistent multiple would be expected if they were related. Additionally, in a previous stack (King & Bell 1997) the I_2W_1 seabed multiple was clearly visible; however, subsequent processing has successfully removed this multiple train. It is expected that some residual multiple energy survives, reducing the coherency of the low-amplitude primary reflectors.

Table 1. Data processing scheme applied to multifold seismic reflection data.*

Process	Domain	Target
Pre-stack		
Mute	CSP	Air wave, secondary event, tide crack and ground roll (surface-coupled shear wave)
True amplitude recovery	CSP	Attenuation and spherical divergence
Bandpass filter	CSP	Signal bandwidth, geophone resonance
Predictive deconvolution	CO	Ice-layer multiple
Ray-path integral moveout	CMP	Moveout
Dip moveout	CO	Dip moveout
Bandpass filter	CMP	Process noise
Mute	CMP	Pre-stack, *S–P–S* phase conversion
Stack (RMS, weighted)	CMP	Ice-layer multiple, signal-to-noise ratio
Post-stack		
FD time migration	CMP	Diffraction energy, temporal resolution
Trace display	CMP	Display balancing

* CSP, common shot point; CO, common offset; CMP, common midpoint.

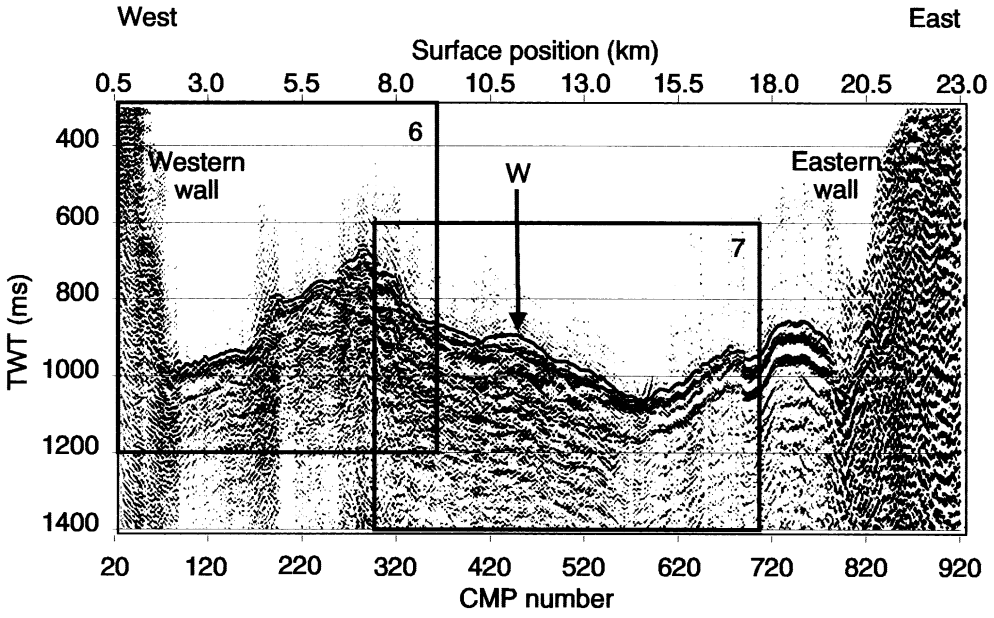

Figure 5. Seismic reflection section crossing George VI Sound from the foot of the Uranus Glacier in the west to the Batterbee Mountains in the east (line T in Fig. 2 inset). The rectangles show the extent of Figs 6 and 7. The vertical exaggeration at CMP 600 is approximately 12:1 at the seabed. W marks the position of the walkaway experiment.

Table 2. Apparent refraction velocities and time intercepts from walkaway experiment.

Phase	Velocity (km s^{-1})	Zero-offset time (ms)
RF1	3.99 ± 0.02	759.6 ± 0.8
HD2	4.83 ± 0.01	876.0 ± 2.0
HD3	5.23 ± 0.01	1024.0 ± 4.0
HD4	5.42 ± 0.01	1105.0 ± 5.0
HD5	5.96 ± 0.01	1516.0 ± 3.0

SU3 comprises a broad band of subparallel reflectors of uniform amplitude. The unit is seen 50–100 ms TWT below the seabed reflection and is recognizable over a 200–250 ms TWT thickness. The reflectors have a shallow eastward dip on a time section west of the bathymetric high at kilometre 7.1. The apparent dip is reversed on the eastern flank of the horst. Assuming an overburden velocity of 2.6 km s^{-1}, these events dip less than 5° east. The SU3 internal reflectors are displaced on by several normal faults. The faults dip west on the western flank of the horst, and east on the eastern flank. The faulting seen in SU3 appears to disrupt reflector continuity in SU1 only in the vicinity of the eastern boundary fault of the graben. The graben bounding faults have dips of approximately 40°, and exhibit the largest observable throws; the eastern fault displays a minimum throw of approximately 220 m, assuming an overburden velocity of 2.6 km s^{-1}.

East of the horst the seabed dips gently (approximately 1.4° east) towards the deepest point of the traverse (14.5 km), 885 m below sea level (Fig. 7). Two lenses assigned to SU1 are seen below the seabed reflection. These lenses have a maximum time thickness of 50 ms TWT. The eastern lens grades into a pod of strong seabed-parallel reflectors which fill in the central trough to a limited horizontal extent. Reflectors similar to

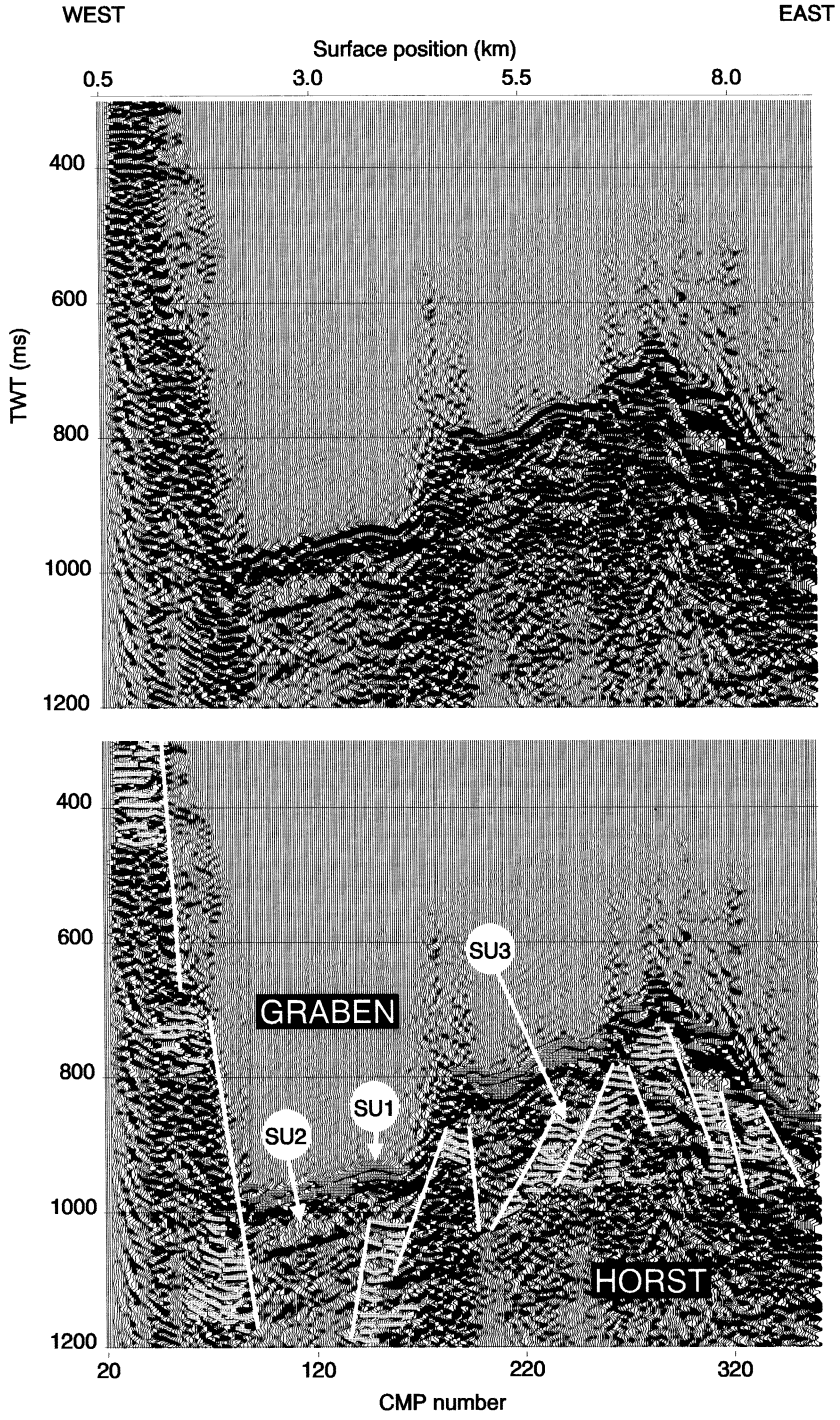

Figure 6. Seismic reflection section over horst and graben features on the western side of the Sound. In SU1 the prominent reflectors are highlighted by dark grey shading in the lower part of the figure. In SU3 the prominent reflectors are highlighted by light grey shading and interpreted faults are marked by solid white lines.

SU3 dip west beneath small pockets of SU2. The SU3 reflections are truncated by medium-angle normal faulting that does not appear to penetrate the overlying material.

The SU3 reflectors are similar in character to those seen in the western boundary wall; both sets consist of discontinuous subparallel reflectors of similar amplitude, spatial frequency and interval velocity. The reflectors are of a type expected from a sedimentary succession of interbedded sandstones and shales. We equate both groups and interpret SU3 as representing FBG rocks which are known to border the western margin of GVIS in this locality. Refraction velocity data support this interpretation (Section 2.2.2), suggesting that the rocks of the FBG extend at least as far east as kilometre 8 (Fig. 6), and possibly up to the bathymetric low.

East of the bathymetric trough a change in seismic character occurs. A strong seabed primary reflection is underlain by a non-reflective zone, which we label as SU4 (Fig. 7). The subseabed section is overprinted by three phases. The first,

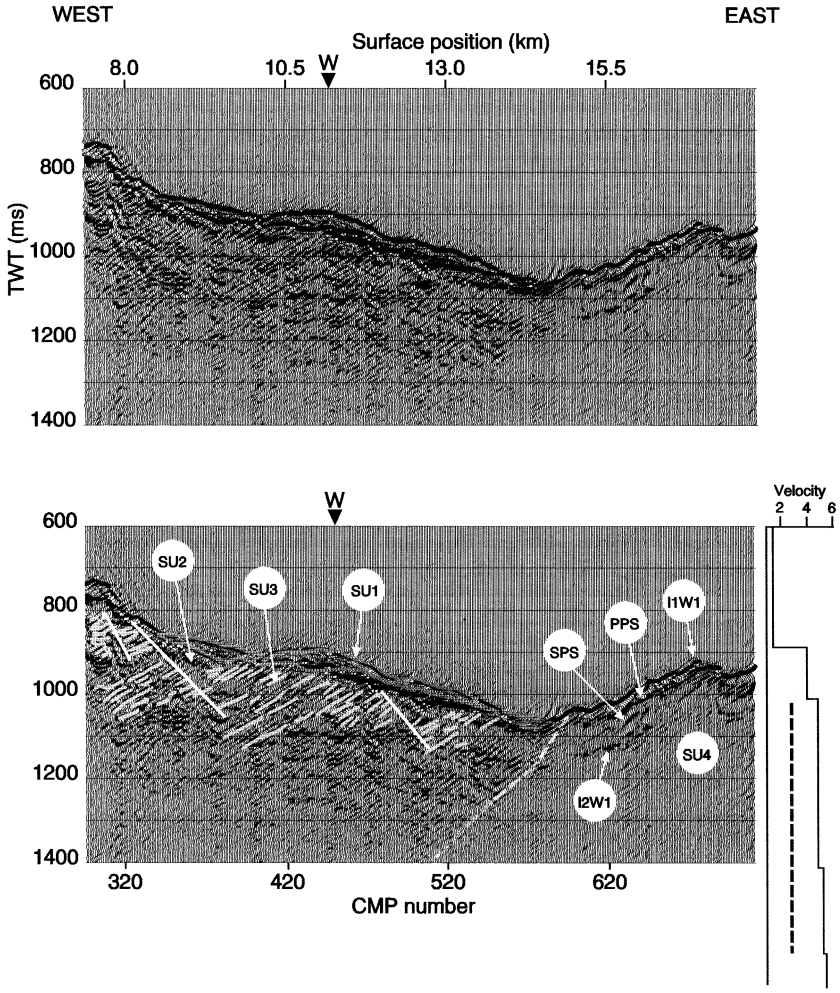

Figure 7. Seismic reflection section over bathymetric low in the centre of George VI Sound. In SU1 the prominent reflectors are highlighted by dark grey shading; in SU3 the prominent reflectors are highlighted by light grey shading. Interpreted faults are marked by white lines and the contact between SU3 and SU4 is marked by a dashed white line. SPS and PPS, converted phases (see text); I1W1, seabed primary reflection; I1W2, ice-layer multiple. W marks the position of the walkaway experiment. An interval velocity function interpreted from the walkaway experiment is displayed at the same two-way timescale as the reflection record. The dashed line indicates the position and the time thickness of units interpreted as the Fossil Bluff Group.

occurring 44 ms after the seabed primary, is the *P–P–S* wave conversion of the seabed primary at the base of the ice shelf. This phase is shortly followed by the second, an *S–P–S* converted phase. The third phase arrives 90 ms after the seabed primary and is the first seabed *P*-wave ice multiple (I_2W_1). The stronger coherency seen on the eastern side of the Sound is due to the combination of a hard seafloor supplying more reflected incident energy to the primary and secondary phases and the absence of any subseabed reflectors.

The disrupted seabed topography east of the bathymetric low is probably the surface expression of further normal faulting. The eastern border of the Sound is marked by a narrow trough, less than one kilometre in width, adjacent to a steep boundary wall (Fig. 5). The topography of the bordering block is not imaged at early TWT (shallow depths). The eastern wall may mark the position of a bounding fault. The steep boundary faults and narrow rift walls on both sides of the Sound are typical of transtensional basins and are similar to those seen on the margins of the southern Dead Sea basin (ten Brink & Ben-Avraham 1989; Csato *et al.* 1997).

Table 3. Assignment of walkaway units to identified seismic units (interpreted depths from walkaway modelling).

Walkaway phase	Velocity (km s^{-1})	Thickness (m)	Walkaway unit	Seismic unit
RF1	3.99	270	WU1	SU2
HD2	4.83	950	WU2	SU3
HD3	5.23	510	WU3	SU3
HD4	5.42	2100	WU4	SU4
HD5	5.96	–		

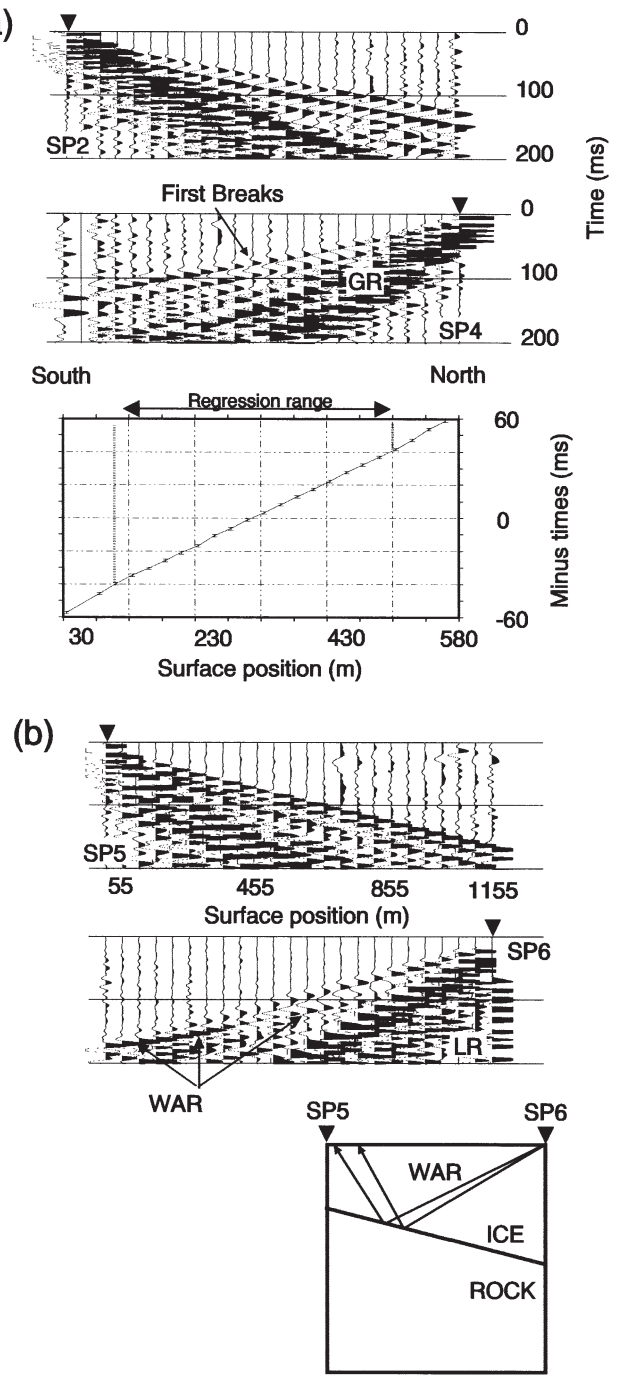

Figure 8. (a) Refraction shot records showing first breaks from shots 2 and 4 of line 1, parallel to scarp wall (for location reference see Fig. 2). GR, ground roll. Graph shows 'minus time' range used in *P*-wave velocity regression calculation from reversed refractor coverage of line 1. (b) Shot records 5 and 6 from line 2, orthogonal to the scarp wall. Shot record 6 records a wide-angle reflection (WAR) arrival at far offsets. Linear reflectors (LR) are identified at near offsets. The cartoon shows the interpreted bedrock interface giving rise to the WAR.

2.2.2 *Refraction data*

In the 1996/7 summer field season a refraction experiment to determine an *in situ* compressional wave velocity for the FBG was undertaken adjacent to the Fossil Bluff ski-way (Fig. 2).

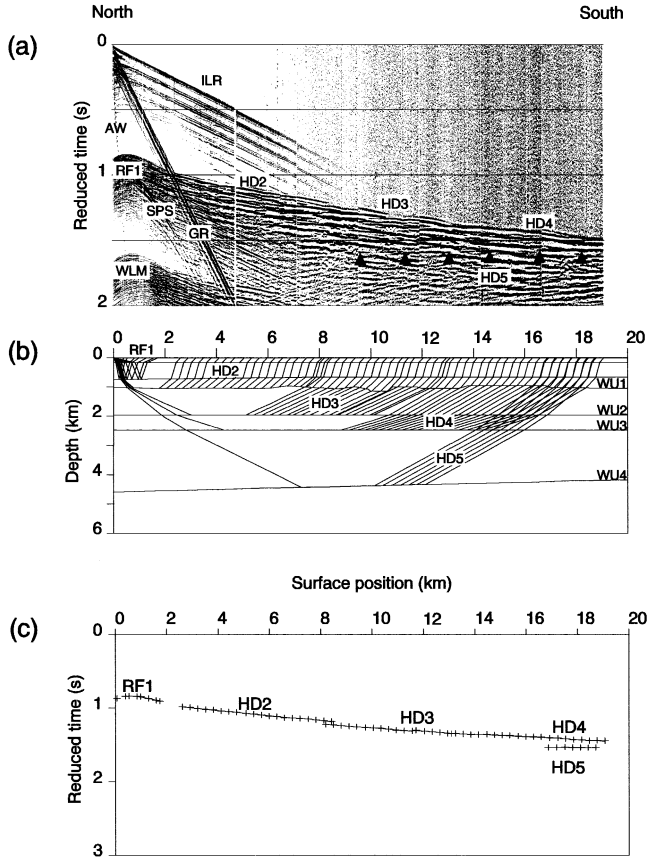

Figure 9. (a) Reduced-time plot of data from the walkaway reflection/refraction experiment bisecting George VI Sound (reduction velocity 6.0 km s^{-1}). See Tables 1 and 2 for apparent velocity and interpreted unit thicknesses of picked phases. Black triangles mark the position of the secondary arrival HD5. AW, air wave; GR, ground roll; SPS, seabed reflection converted phase; WLM, seabed reflection water-layer multiple; ILR, ice-layer refraction and reflection multiple train. (b) Ray tracing of the walkaway experiment; the phase arrivals were modelled as head waves and wide-angle reflections using RAYINVR (Zelt & Smith 1992). RF1 and HD2–HD5 indicate modelled ray paths to and from these reflecting/refracting interfaces. (c) Reduced-time plot showing arrival times of the modelled phases (crosses) overlaid on observed traveltime phase picks (solid line) (reduction velocity 6.0 km s^{-1}).

Reversed refraction records from a line parallel to the rock wall show two first-break phases (Fig. 8a). At short offsets, less than 80 m, the direct wave arrives first, whilst beyond 80 m the first arrivals are refractions from within the rock wall. The reversed first arrivals from the rock refraction were reduced using the Plus–Minus method (Hagedoorn 1959). Linear regression of the 'minus times' yields an *in situ P*-wave velocity for the FBG rocks of 5.18 ± 0.04 km s^{-1}, where the uncertainty is ± 2 standard deviations.

Fig. 8(b) shows the shot records from the orthogonal line (line 2). A wide-angle reflection (WAR) phase arrives after the ice-layer direct wave over the far offsets on shot record 6. Modelling suggests these reflections arise from an eastward-dipping down-faulted block under the ski-way. At near offsets, closely spaced reflections (LR) of uniform amplitude are evident; they are similar in character to those inferred as due to the FBG on the main seismic reflection section.

The walkaway experiment data collected in 1995/6 are

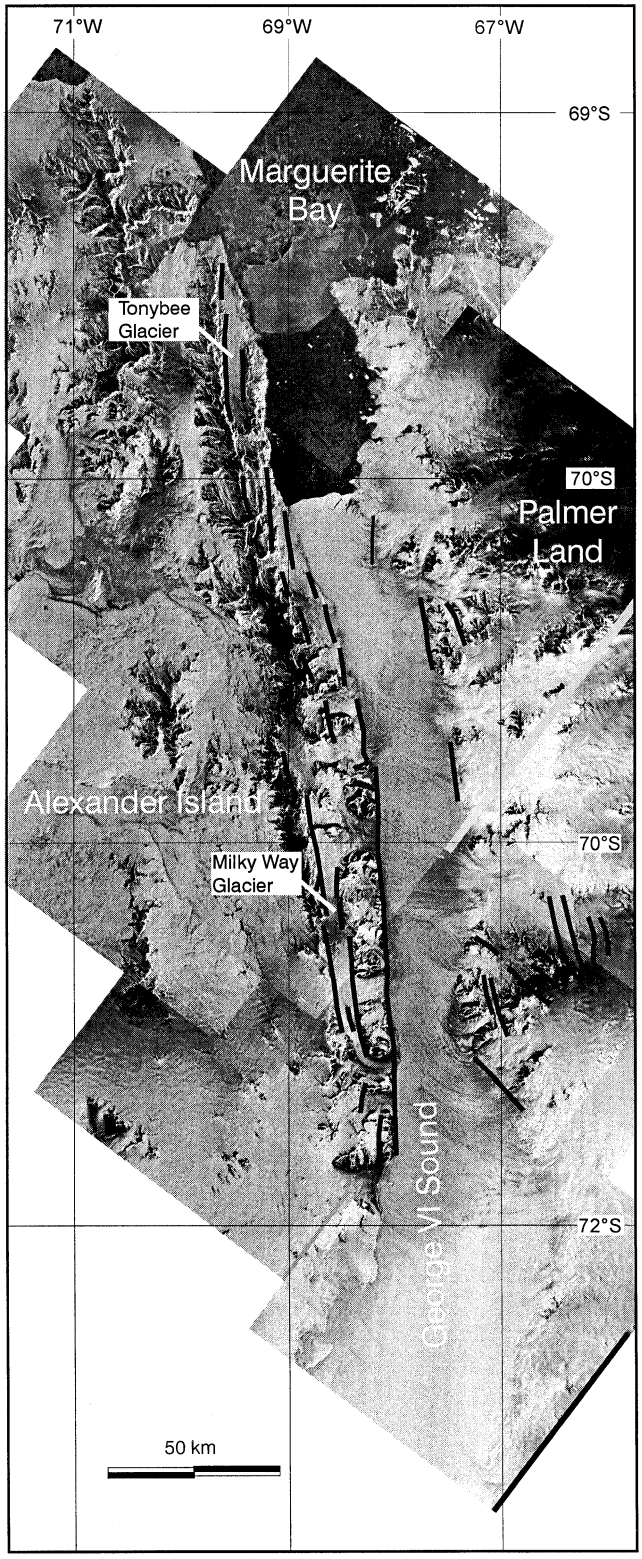

Figure 10. Synthetic-aperture radar image of the northern arm of George VI Sound compiled from ERS-1 satellite data. The bold black lines mark lineaments interpreted as fault traces.

presented in Fig. 9(a), and in King & Bell (1997). At close offsets, subseabed refraction phases arrive after ice-shelf direct and refracted reverberations; they are much stronger than the weak ice-layer reverberations and are easily identified. At far offsets the refractions comprise true first breaks. Three refracted first-arrival phases are identified: HD2, HD3 and HD4. One secondary phase arrival is evident, about 100 ms after the first breaks at the furthest offsets (Fig. 9a). Table 2 presents the zero-offset times and apparent velocities for these phases.

Owing to the absence of shot-reversed coverage, modelling was restricted to head wave generation for a simple plane-layer velocity model (Figs 9b and c). Constant-velocity layers were assumed. A slight southerly dip of the seabed of less than 1° accommodates the observed offset apex of the RF1 reflection hyperbola. Modelling suggests the seabed generates a section of postcritical-angle reflection before being overtaken by the refracted phase HD2; the crossover is obscured by the ground roll (GR).

The HD2 apparent velocity varies with offset and is attributed to refractor topography; the phase is assigned the slowest velocity, with the variations modelled as topographic changes. Variations in the arrival times of deeper refractions are also accommodated by topographic variation on this boundary. Using the slowest apparent velocity for the HD2 phase engenders a minimum thickness for WU1 and WU2, and minimizes topography on the HD2 refractor. The apparent velocity variation on the HD2 refractor indicates substantial thickness changes in WU1, and may denote the presence of faulting or slumping. The refractor phases of HD3 and HD4 are modelled using horizontal layers, while HD5 has a 2° northerly dip.

The *in situ* refraction velocity of 5.18 km s^{-1} for FBG rocks from the ski-way experiment is in close agreement with the HD3 phase velocity. The apparent velocities for the HD2 phase have a wide spread but have a mean value close to 5.1 km s^{-1}, and so for simplicity of interpretation HD2 will also be considered indicative of FBG rocks. This hypothesis supports the interpretation of the steeply dipping reflections in the centre of the Sound as emanating from FBG rocks. Assigning both HD2 and HD3 phases as refractions from FBG rocks (SU3) gives a total group thickness of 1460 m at a location midway across the Sound (see Table 3).

SU1 and SU2 are constrained by this interpretation to be represented by WU1. If we infer that SU1 represents a young, glacially derived drape deposited in lenses of limited extent, then the low density and seismic velocities characteristic of such deposits (Morgan 1969; Barret & Froggat 1978) explain the lack of a refracted arrival from such a layer underlying an ice shelf. This leaves WU1 equated to SU2, representing a consolidated marine or glacial deposit infilling the topography of the horst and graben.

The bathymetric low forms the boundary between the reflective subseabed of the western side of the Sound and the seismically opaque eastern margin. The change in character could be caused by a non-reflective seismic facies, intense deformation or the absence of soft sediment cover. The marked increase in seabed reflection strength east of the low indicates a hard seafloor lithology of high acoustic impedance. WU4, with a *P*-wave velocity of 5.4 km s^{-1}, is a likely candidate for the seafloor lithology (SU4). For this unit to crop out at the bathymetric low, from 1.73 km depth below the seabed at the walkaway location, a westerly dip of 19° is required on the contact between SU3 and SU4. This contrasts with an apparent westerly dip of 11° (for an assumed overburden velocity for SU1 and SU2 of 2.6 km s^{-1}) of the SU3 reflectors. We infer that an unconformable contact between SU3 and SU4 must

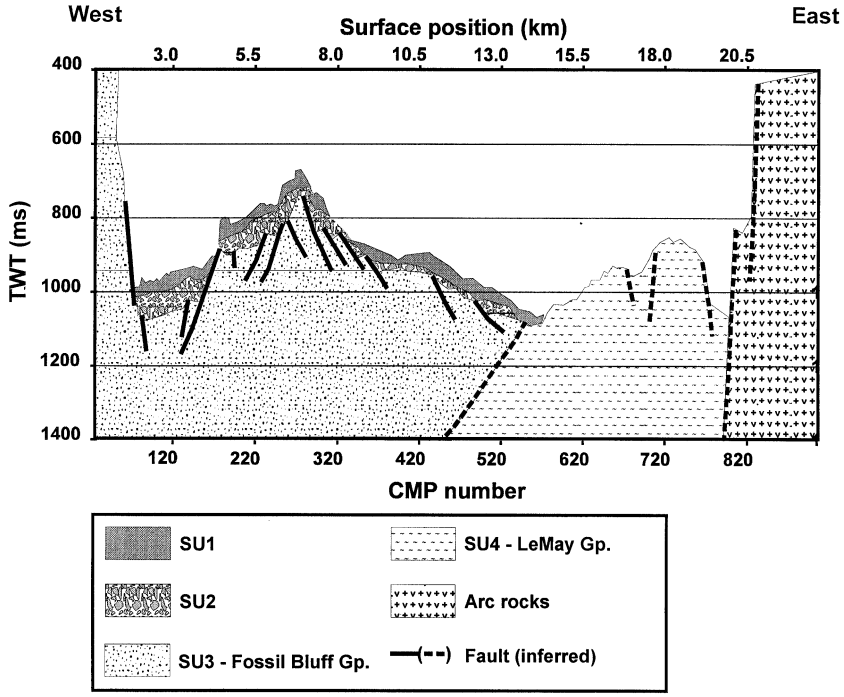

Figure 11. Interpretation of the seismic section across George VI Sound shown in Fig. 5 (line T in Fig. 2 inset). The eastern wall of the Sound marks an inferred faulted contact between LMG rocks to the west and arc-related rocks to the east. Picked faults shown as solid black lines, and inferred faults and contacts as broken black lines.

exist to accommodate the difference in dip, SU3 onlapping SU4 until pinching out at the bathymetric low (Fig. 7). This necessitates an older age for SU4 than the ?Bathonian/Kimmeridgian to Albian ages of the FBG (SU3). The smooth negative magnetic anomaly over Alexander Island and the Sound suggest a continuation of the LMG and FBG rocks below the Sound, and therefore we correlate SU4 with the LMG rocks. The sharp positive anomaly on the eastern border of the Sound suggests the LMG rocks come into faulted contact with batholithic rocks giving rise to the PMA (Renner *et al.* 1985).

2.3 Synthetic-aperture radar

Fig. 10 is a synthetic-aperture radar image of the northern arm of GVIS. The mosaic is compiled from subsampled images from the ERS-1 satellite and has an effective pixel resolution of 30 m. The high, linear mountain ranges of eastern Alexander Island contrast markedly with the more scattered outcrops of western Palmer Land, emphasizing that there is strong topographic asymmetry across the Sound.

There are a number of lineaments on the image, associated with the following features:

(1) the western margin of George VI Sound, as a continuous lineament in the central part and a series of en-echelon features in the northernmost part;

(2) the edges of north–south orientated glaciers in eastern Alexander Island, most notably the Tonybee and Milky Way Glaciers;

(3) short sections of the eastern margin of the Sound and some glacier margins and scarps in western Palmer Land.

We interpret these lineaments as fault traces. The asymmetry of the fault pattern and the topography suggest that this is an early-stage rift in which the dominant structures are half-graben, similar to the Southern Main Ethiopian Rift (e.g. Hayward & Ebinger 1996). Thus the bounding fault of the main basin is aligned along the western side of the Sound and the other lineaments identified on the radar image and the seismic line are antithetic and secondary faults. The high topographic relief on the bounding fault of the basin results from flexural warping due to unloading of the footwall block during rifting (Kusznir, Marsden & Egan 1991).

The length of faults bounding a rift are an indication of the effective elastic thickness of the crust at the time of rifting (Hayward & Ebinger 1996). In general, long faults develop in the early stages of rifting when relatively thick, cold crust is being ruptured. There are faults bordering George VI Sound with lengths ranging from 50 to 100 km, which suggests that these are the early, primary fault scarps of the half-graben.

3 DISCUSSION

The seabed topography across the traverse is similar to that reported by Crabtree *et al.* (1985), from a plumb-line survey carried out at the northern ice front of the Sound (Fig. 2), and to that obtained from seismic soundings acquired over the ice sheet by Maslanyj (1987). This may indicate the continuation of extensional structures along the length of the northern arm of the Sound. To the south of the location of the experiment the seabed profiles (Maslanyj 1987) retain their characteristic 'W' shape on the western flank of the Sound. However, they show an additional raised block on the southern end of the

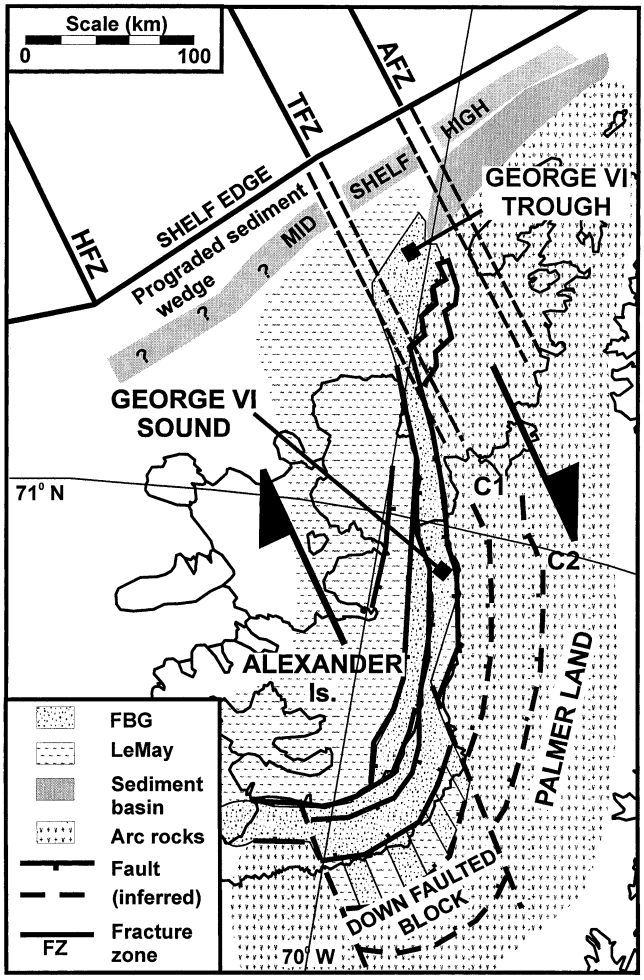

Figure 12. Cartoon map of the Alexander Island region indicating the major known and inferred tectonic features. The arrows indicate the major dextral transtensional stress field existing in the period between 50 and 30 Ma. AFZ, TFZ and HFZ: Adelaide, Tula and Heezen fracture zones, respectively. C1 and C2 are major faults interpreted from radio echo-soundings (Crabtree *et al.* 1985).

eastern border. Fig. 12 presents fault traces inferred from breaks in slope on these seabed profiles.

Crabtree *et al.* (1985) interpreted two fault zones running parallel to the northeastern border of the Sound and proposed the continuation of these faults south into the Goodenough Glacier area (Fig. 12). The eastern fault (C2 in Fig. 12) marks the inferred position of the western escarpment of the Palmer Land plateau. The southern extrapolation of fault C1 intersects the eastern boundary of the Sound at the point where it widens to the south. The fault traces appear to delineate positions of downthrown fault blocks. The lack of relief and the scarcity of nunataks in this area support the hypothesis of underlying downthrown fault-bounded blocks. Magnetic data show that the PMA follows the eastern boundary as the Sound widens to the south (Fig. 1).

The low topographic relief on the bordering escarpment faults of the southern Sound, combined with the larger rift width of 80–100 km, is indicative of a full graben structure similar to the Central Main Ethiopian and Eastern-Central Afar Rifts (Hayward & Ebinger 1996).

The rift forming the Sound has opened along the trend of the western margin of the Antarctic Peninsula batholith. This suggests that rifting has been controlled either directly by thermal weakening and uplift of the lithosphere associated with emplacement of this batholith or by reactivation of a relict suture, possibly related to earlier docking of accretionary slivers in a fore-arc location.

3.1 Cause of rifting

Although there is little evidence of non-subduction-related volcanic and intrusive rocks on Alexander Island, Hole (1988) described a suite of alkali volcanic rocks which post-date the cessation of subduction by 18–30 Myr. He attributed the delay in eruption of these volcanic rocks, following the cessation of subduction, to the need to remove or make permeable the subducted lithosphere before the magma was able to surface. Similarly, McCarron & Larter (1998) attribute andesitic lavas seen in northern Alexander Island (approximately 53 Ma) and at Stacatto Peaks (approximately 75 Ma) in the south (Fig. 2) to slab windows created in separate ridge crest subduction events prior to termination of subduction at the palaeotrench by collision with the Antarctic–Phoenix ridge. The lack of evidence of major thermal events subsequent to the cessation of subduction favours a rifting mechanism of the fore-arc lithosphere related to stress and thermal weakening induced by a protracted period of subduction.

We describe a possible interpretation of the mid-Cretaceous to early Tertiary subduction history of the area, focusing on the formation of the rift observed in eastern Alexander Island and GVIS. Following and possibly coeval with deposition of the youngest FBG sediments, the FBG sediments were uplifted and deformed in a dextral transpressive stress regime related to oblique subduction between the Heezen and Tharp fracture zones (Nell & Storey 1991), accounting for the early thermal history recorded in zircon fission track data (Fig. 13a). An early-Tertiary rotation of subduction angle followed by a reduction in subduction rate resulted in trench retreat, creating tensional stresses in the accretionary prism and fore-arc basin (Storey *et al.* 1996; McCarron & Larter 1998). Thermal weakening of the fore-arc lithosphere due to contemporaneous early Tertiary (50–30 Ma) arc magmatism in Palmer Land and Alexander Island (McCarron & Millar 1997) combined with the tensional stress produced the ideal regime for rifting between Alexander Island and the Antarctic Peninsula (Fig. 13b).

The oblique orientation of the northern Sound with respect to the stress regime gave rise to dextral transtension (Fig. 12), evidence of which is seen within the FBG as displaced transpressional thrusts and sandstone dykes (Storey & Nell 1988). At Giza Peak and Belemnite Point (Fig. 2), faulted margins of an Eocene calc-alkaline dyke indicate that dextral transtensional deformation affected the fore-arc until the late middle Eocene (D. I. M. Macdonald & I. L. Millar, personal communication 1997). Strain was accommodated primarily by dextral strike-slip motion on bounding faults (Storey & Nell 1988) with a minor component of normal extension.

In the southern segment of the Sound an orthogonal geometry between the Sound and the stress regime gave rise to predominantly normal extension. More pronounced extension in the south of the Sound (Maslanyj 1991) may have caused depression of blocks of the PMA batholith on the western border of Palmer Land. Positive magnetic anomalies

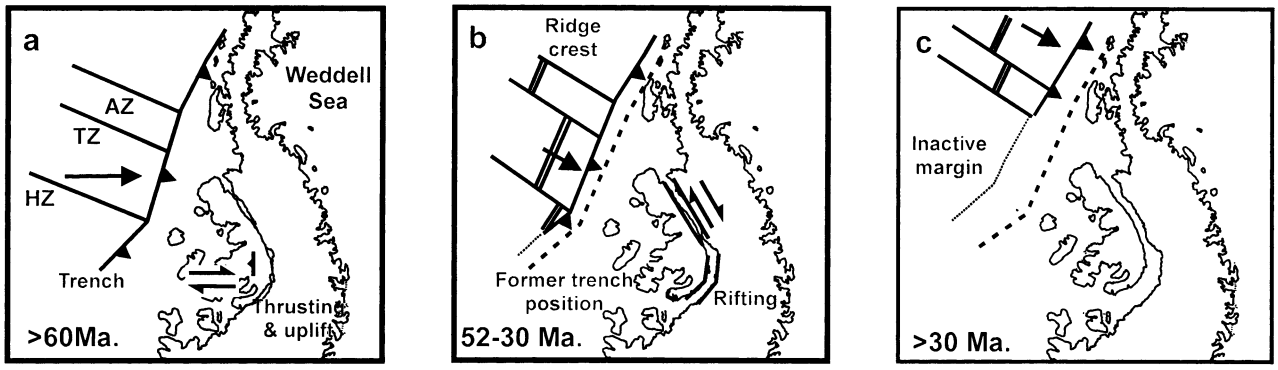

Figure 13. (a) Dextral transpression in the fore-arc due to oblique subduction. HZ, TZ and AZ: Heezen, Tula and Adelaide fracture zones. The single arrow in each part of the figure indicates the subduction direction and its length indicates the subduction rate. (b) Spreading-rate reduction leads to trench retreat and transtension in the fore-arc. Rifting initiated in George VI Sound. (c) Antarctic–Phoenix ridge crest collisions with trench lead to progressive cessation of subduction and removal of rifting stress.

(Maslanyj *et al.* 1991) may mark the presence of incipient axial volcanism similar to the East African Rift (Hayward & Ebinger 1996).

The predominantly half-graben strike-slip structures in the north of the Sound compared with the full-graben normal faulting in the south suggest rift segmentation, with the position of an 'intersegment accommodation zone' (Hayward & Ebinger 1996) inferred in the vicinity of the Goodenough Glacier.

Collision of successive ridge crest segments with the trench (44 Ma in the south and 30 Ma in the north) led to a progressive cessation of subduction, removing tensional stresses in the fore-arc and halting further rifting (Fig. 13c). The collision uplifted the fore-arc and is recorded as a period of accelerated denudational cooling noted in the apatite fission track record (Storey *et al.* 1996).

3.2 Cenozoic sedimentation

The trough created by rifting formed a primary depositional centre for sediments from Alexander Island and Palmer Land. Glacial deposits on the Batterbee plateau (Clapperton & Sugden 1982) indicate the former presence of an ice mass large enough to inundate the Sound, whilst contemporary motion indicators record a northerly transport direction. The resulting ice stream would have entrained soft sediment deposits in the Sound, redepositing them in George VI Trough (Marguerite Bay area) and over the shelf edge. A negative Bouguer anomaly over the Trough is attributed to the presence of sediments (Johnson 1997). Any soft sediments deposited in the Sound prior to the final glacial inundation were probably removed by scouring, therefore we propose a syn-glacial origin for SU2. The chaotic nature of the unit is in line with the deposition of till infill in voids at the base of an ice stream traversing a rough rock-head topography. An age prior to the last major glacial maximum (Wisconsin) is likely.

Flow lines over the ice shelf show that ice from the large Palmer Land glaciers engulfs the Sound (Fig. 10) (Reynolds 1981; Reynolds & Hambrey 1988). Sugden & Clapperton (1981) propose a regional non-depositional sub-ice-shelf environment, entrained material being removed by deposition in ice-cored moraines on the western border of the Sound by ablation and thrusting processes (Clapperton & Sugden 1983). The absence of a postglacial drape over the western margin of the Sound supports this proposal. An anomaly in the ice flow pattern marks the encroachment of the Uranus Glacier into the Sound (Fig. 10) (Sugden & Clapperton 1981; Reynolds & Hambrey 1988). We suggest that SU1 represents a locally confined sediment drape derived from entrained material from the Uranus Glacier. If this interpretation is correct, then the drape has been deposited since the last major glacial inundation in the Wisconsin, so we suggest a Quaternary age for the unit.

4 CONCLUSIONS

Graben and horst structures below the Sound indicate an extensional origin. The most probable age for rifting was between 50 and 30 Ma, corresponding to a period of high thermal and tensional stress in the Antarctic Peninsula fore-arc associated with subduction. The Antarctic Peninsula batholith appears to have controlled the location of rifting in the fore-arc. Asymmetry between the northern and southern segments of the rift suggests segmentation, possibly related to ridge segmentation. This interpretation emphasizes the importance of ridge segmentation, subduction orientation and spreading-rate history over the tectonic evolution of a fore-arc terrain.

Seismic units and velocity–depth analyses combined with aeromagnetic data suggest the Sound is underlain by rocks of the LeMay and Fossil Bluff Groups in unconformable contact. These rocks are in faulted contact with volcanic and plutonic rocks of the Mesozoic arc on the eastern border of George VI Sound.

Possible syn- and postglacial Cenozoic deposits are seen overlying graben and horst blocks composed of FBG rocks.

ACKNOWLEDGMENTS

We wish to thank D. I. M. Macdonald and I. L. Millar for useful discussions and access to manuscripts, B. C. Storey and A. P. M. Vaughan for discussion and review of geological interpretations, and A. M. Reading, N. Boyd, P. Ramsbottom, P. Thomson and S. Waters for their help during field work. Two journal referees provided valuable comments on the manuscript.

REFERENCES

Ayling, M.E., 1984. The geology of parts of central west Palmer Land, *Br. Antarctic Survey Scientific Reports,* **105,** 1–60.

Barker, P.F., 1982. The Cenozoic subduction history of the Pacific margin of the Antarctic Peninsula: ridge crest–trench interactions, *J. geol. Soc. Lond.,* **139,** 787–801.

Barret, P.J. & Froggat, P.C., 1978. Densities, porosities, and seismic velocities of some rocks from Victoria Land, Antarctica, *NZ J. Geol. Geophys.,* **21,** 175–187.

Beaudoin, B.C., ten Brink, U.S. & Stern, T.A., 1992. Characteristics and processing of seismic data collected on thick, floating ice: results from the Ross Ice Shelf, Antarctica, *Geophysics,* **57,** 1359–1372.

Burn, R.W., 1984. The geology of the Lemay Group, Alexander Island, *Br. Antarctic Survey Scientific Reports,* **109,** 1–65.

Butterworth, P.J., Crame, J.A., Howlett, P.J. & Macdonald, D.I.M., 1988. Lithostratigraphy of Upper Jurassic–Lower Cretaceous strata of eastern Alexander Island, *Cretaceous Res.,* **9,** 249–264.

Cande, S.C., Herron, E.M. & Hall, B.R., 1982. The Early Cenozoic tectonic history of the southeast Pacific, *Earth planet. Sci. Lett.,* **57,** 63–74.

Clapperton, C.M. & Sugden, D.E., 1982. Late Quaternary glacial history of George VI Sound area, West Antarctica, *Quaternary Res.,* **18,** 243–267.

Clapperton, C.M. & Sugden, D.E., 1983. Geomorphology of the Ablation Point massif, Alexander Island, Antarctica, *Boreas,* **12,** 125–135.

Crabtree, R.D., Storey, B.C. & Doake, C.S.M., 1985. The structural evolution of George VI Sound, Antarctic Peninsula, *Tectonophysics,* **114,** 431–442.

Csato, I., Kendall, C.G.St.C., Nairn, A.E.M. & Baum, G.R., 1997. Sequence stratigraphic interpretations in the southern Dead Sea basin, Israel, *Geol. Soc. Am. Bull.,* **109,** 1485–1501.

Culshaw, N.G., 1975. The geology of Carse Point, Palmer Land, *Br. Antarctic Survey Bull.,* **41,** 23–30.

Doubleday, P.A., Macdonald, D.I.M. & Nell, P.A.R., 1993. Sedimentology and structure of the trench-slope to forearc basin transition in the Mesozoic of Alexander Island, Antarctica, *Geol. Mag.,* **130,** 737–754.

Fleming, W.L.S., Stephenson, A., Roberts, B.B. & Bertrum, G.C.L., 1938. Notes on the scientific work of the British Graham Land expedition, 1934–1937, *Geograph. J.,* **91,** 508–532.

Garrett, S.W., 1990. Interpretation of reconnaissance gravity and aeromagnetic surveys of the Antarctic Peninsula, *J. geophys. Res.,* **95,** 6759–6777.

Grant, F.S. & West, G.F., 1965. *Interpretation Theory in Applied Geophysics,* pp. 133–134, McGraw-Hill, Toronto.

Hagedoorn, J.G., 1959. The Plus–Minus method of interpreting seismic refraction sections, *Geophys. Prospect.,* **7,** 158–182.

Hayward, N.J. & Ebinger, C.J., 1996. Variations in the along-axis segmentation of the Afar Rift system, *Tectonics,* **15,** 244–257.

Holdsworth, B.K. & Nell, P.A.R., 1992. Mesozoic radiolarian faunas from the Antarctic Peninsula: age, tectonic and palaeoceanographic significance, *J. geol. Soc. Lond.,* **149,** 1003–1020.

Hole, M.J., 1988. Post-subduction alkaline volcanism along the Antarctic Peninsula, *J. geol. Soc. Lond.,* **145,** 985–998.

Jarvis, E.P. & King, E.C., 1993. The seismic wavefield recorded on an Antarctic ice shelf, *J. seism. Explor.,* **2,** 69–86.

Johnson, A.C., 1997. Cenozoic tectonic evolution of the Marguerite Bay area, Antarctic Peninsula, interpreted from geophysical data, *Antarctic Sci.,* **9,** 268–280.

King, L., 1964. Pre-glacial geomorphology of Alexander Island, in *Antarctic Geology,* pp. 53–64, ed. Adie, R.J., North-Holland, Amsterdam.

King, E.C. & Bell, A.C., 1995. New seismic data from the Ronne Ice Shelf, Antarctica, in *Weddell Sea Tectonics and Gondwana Break-up,* eds Storey B.C., King E.C. & Livermore, R.A., *Geol Soc. Lond. Spec. Publ.,* **108,** 213–226.

King, E.C. & Bell, A.C., 1997. Seismic reflection investigation of George VI Sound, Antarctic Peninsula, in *The Antarctic Region: Geological Evolution and Processes,* pp. 697–704, ed. Ricci, C.A., Università di Siena, Siena.

Kusznir, N.J., Marsden, G. & Egan, S.S., 1991. A flexural-cantilever simple-shear/pure-shear model of continental lithosphere extension: applications to the Jeanne d'Arc Basin, Grand Banks and Viking Graben, North Sea, in *The Geometry of Normal Faults,* eds Roberts, A.M., Yielding, G. & Freeman, B., *Geol Soc. Lond. Spec. Publ.,* **56,** 41–60.

Larter, R.D., Rebesco, M., Vanneste, L.E., Gamboa, L.A.P. & Barker, P.F., 1997. Cenozoic tectonic, sedimentary and glacial history of the continental shelf west of Graham Land, Antarctic Peninsula, in *Geology and Seismic stratigraphy of the Antarctic margin*, **2**. Antarctic Research Series volume 71, pp. 1–28, eds Barker, P.F. & Cooper, A.K. American Geophysical Union, Washington D.C.

Leat, P.T. & Scarrow, J.H., 1994. Central volcanoes as sources for the Antarctic Peninsula Volcanic Group, *Antarctic Sci.,* **6,** 365–374.

Leat, P.T., Scarrow, J.H. & Millar, I.L., 1995. On the Antarctic Peninsula batholith, *Geol. Mag.,* **132,** 399–412.

Maslanyj, M.P., 1987. Seismic bedrock depth measurements and the origin of George VI Sound, Antarctic Peninsula, *Br. Antarctic Survey Bull.,* **75,** 51–65.

Maslanyj, M.P., 1991. Geophysical investigation of George VI Sound, Antarctic Peninsula, in *Geological Evolution of Antarctica,* pp. 527–530, eds Thomson, M.R.A., Crame, J.A. & Thomson, J.W., Cambridge University Press.

Maslanyj, M.P., Garrett, S.W., Johnson, A.C., Renner, R.G.B. & Smith, A.M., 1991. Aeromagnetic anomaly map of West Antarctica (Weddell Sea sector), *BAS GEOMAP Series,* Sheet 2, British Antarctic Survey, Cambridge.

McCarron, J.J. & Larter, R.D., 1998. Late Cretaceous to early Tertiary subduction history of the Antarctic Peninsula, *J. geol. Soc. Lond.,* **155,** 255–268.

McCarron, J.J. & Millar, I.L., 1997. The age and stratigraphy of fore-arc magmatism in Alexander Island, Antarctica, *Geol. Mag.,* **134,** 507–522.

Moncrieff, A.C.M. & Kelly, S.R.A., 1993. Lithostratigraphy of the uppermost Fossil Bluff Group (Early Cretaceous) of Alexander Island, Antarctica: history of an Albian regression, *Cretaceous Res.,* **14,** 1–15.

Morgan, N.A., 1969. Physical properties of marine sediments as related to seismic velocities, *Geophysics,* **34,** 529–545.

Nell, P.A.R. & Storey, B.C., 1991. Strike-slip tectonics within the Antarctic Peninsula fore-arc, in *Geological Evolution of Antarctica,* pp. 443–448, eds Thomson, M.R.A., Crame, J.A. & Thomson, J.W., Cambridge University Press.

Nichols, R.L., 1953. *Geomorphology of Marguerite Bay, Palmer Peninsula, Antarctica,* Department of the Navy, Office of Naval Research, Washington, DC.

Renner, R.G.B., Sturgeon, L.J.S. & Garrett, S.W., 1985. Reconnaissance gravity and aeromagnetic surveys of the Antarctic Peninsula, *Br. Antarctic Survey Scientific Reports,* **110**.

Reynolds, J.M., 1981. Lakes on George VI Ice Shelf, Antarctica, *Polar Record,* **20,** 425–432.

Reynolds, J.M. & Hambrey, M.J., 1988. The structural glaciology of George VI Ice Shelf, Antarctic Peninsula, *Br. Antarctic Survey Bull.,* **79,** 79–95.

Rowe, P.J., 1973. The geology of the area between Riley and Bertram Glaciers, Palmer Land, *Br. Antarctic Survey Bull.,* **35,** 51–72.

Storey, B.C., Brown, R.W., Carter, A., Doubleday, P.A., Hurford, A.J., Macdonald, D.I.M. & Nell, P.A.R., 1996. Fission-track evidence for the thermotectonic evolution of a Mesozoic–Cenozoic fore-arc, Antarctica, *J. geol. Soc. Lond.,* **153,** 65–82.

Storey, B.C. & Garrett, S.W., 1985. Crustal growth of the Antarctic Peninsula by accretion, magmatism and extension, *Geol. Mag.,* **122,** 5–14.

Storey, B.C. & Nell, P.A.R., 1988. Role of strike-slip faulting in the tectonic evolution of the Antarctic Peninsula, *J. geol. Soc. Lond.,* **145,** 333–337.

Sugden, D.E. & Clapperton, C.M., 1981. An ice-shelf moraine, George VI Sound, Antarctica, *Ann. Glaciol.,* **2,** 135–141.

Taner, M.T. & Koehler, F., 1969. Velocity spectra—digital computer derivation and applications of velocity functions, *Geophysics,* **34,** 859–881.

ten Brink, U.S. & Ben-Avraham, Z., 1989. The anatomy of a pull-apart basin: seismic reflection observations of the Dead Sea basin, *Tectonics,* **8,** 333–350.

Thomson, M.R.A., 1975. Upper Jurassic Mollusca from Carse Point, Palmer Land, *Br. Antarctic Survey Bull.,* **41 & 42,** 31–42.

Tranter, T.H., 1991. Accretion and subduction processes along the Pacific margin of Gondwana, central Alexander Island, in *Geological Evolution of Antarctica,* pp. 437–441, eds Thomson, M.R.A., Crame, J.A. & Thomson, J.W., Cambridge University Press.

Wareham, C.D., Millar, I.L. & Vaughan, A.P.M., 1997. The generation of sodic granite magmas, western Palmer Land, Antarctic Peninsula, *Contrib. Mineral. Petrol.,* **128,** 81–96.

Zelt, C.A. & Smith, R.B., 1992. Seismic traveltime inversion for 2-D crustal velocity structure, *Geophys. J. Int.,* **108,** 16–34.